JACS ARTICLES

Published on Web 10/21/2010

Hysteretic Spin Crossover between a Bisdithiazolyl Radical and Its Hypervalent σ-Dimer

Kristina Lekin,[†] Stephen M. Winter,[†] Laura E. Downie,[‡] Xuezhao Bao,[§] John S. Tse,[||] Serge Desgreniers,[‡] Richard A. Secco,[§] Paul A. Dube,[⊥] and Richard T. Oakley*,[†]

Department of Chemistry, University of Waterloo, Waterloo, Ontario N2L 3G1, Canada, Department of Physics, University of Ottawa, Ottawa, Ontario K1N 6N5, Canada, Department of Earth Sciences, University of Western Ontario, London, Ontario N6A 5B7, Canada, Department of Physics and Engineering Physics, University of Saskatchewan, Saskatoon, Saskatchewan S7N 5E2, Canada, and Brockhouse Institute for Materials Research, McMaster University, Hamilton, Ontario L8S 4M1, Canada

Received August 11, 2010; E-mail: oakley@uwaterloo.ca

Abstract: The bisdithiazolyl radical **1a** is dimorphic, existing in two distinct molecular and crystal modifications. The α-phase crystallizes in the tetragonal space group $P\bar{4}2_1m$ and consists of π-stacked radicals, tightly clustered about $\bar{4}$ points and running parallel to *c*. The β-phase belongs to the monoclinic space group $P2_1/c$ and, at ambient temperature and pressure, is composed of π-stacked dimers in which the radicals are linked laterally by hypervalent four-center six-electron S···S−S···S σ-bonds. Variable-temperature magnetic susceptibility χ measurements confirm that α-**1a** behaves as a Curie−Weiss paramagnet; the low-temperature variations in χ can be modeled in terms of a 1D Heisenberg chain of weakly coupled AFM $S = {}^1/_2$ centers. The dimeric phase β-**1a** is essentially diamagnetic up to 380 K. Above this temperature there is a sharp hysteretic ($T\uparrow = 380$ K, $T\downarrow = 375$ K) increase in χ and χT. Powder X-ray diffraction analysis of β-**1a** at 393 K has established that the phase transition corresponds to a dimer-to-radical conversion in which the hypervalent S···S−S···S σ-bond is cleaved. Variable-temperature and -pressure conductivity measurements indicate that α-**1a** behaves as a Mott insulator, but the ambient-temperature conductivity σ_{RT} increases from near 10^{-7} S cm^{-1} at 0.5 GPa to near 10^{-4} S cm^{-1} at 5 GPa. The value of σ_{RT} for β-**1a** (near 10^{-4} S cm^{-1} at 0.5 GPa) initially decreases with pressure as the phase change takes place, but beyond 1.5 GPa this trend reverses, and σ_{RT} increases in a manner which parallels the behavior of α-**1a**. These changes in conductivity of β-**1a** are interpreted in terms of a pressure-induced dimer-to-radical phase change. High-pressure, ambient-temperature powder diffraction analysis of β-**1a** confirms such a transition between 0.65 and 0.98 GPa and establishes that the structural change involves rupture of the dimer in a manner akin to that observed at high temperature and ambient pressure. The response of the S···S−S···S σ-bond in β-**1a** to heat and pressure is compared to that of related dimers possessing S···Se−Se···S σ-bonds.

Introduction

Neutral radicals are open-shell molecules, and the unpaired electrons found in them are capable, in principle, of acting as carriers of charge[1] and/or sources of magnetic coupling.[2] Interest is therefore growing in the development of radicals as building blocks for single-component electronic, magnetic, and even magnetoelectronic materials.[3] Critical to the pursuit of these ventures, however, is the need to understand the complex relationships between solid-state structure and magnetic and electronic function. For example, the strong charge correlation associated with the half-filled ($f = {}^1/_2$) band structure of an array of weakly interacting radicals gives rise to a large on-site Coulomb potential *U*,[4] as a result of which simple (tight-binding) band theory fails, and such materials fall into Mott insulating

[†] University of Waterloo.
[‡] University of Ottawa.
[§] University of Western Ontario.
[||] University of Saskatchewan.
[⊥] McMaster University.

(1) (a) Haddon, R. C. *Nature* **1975**, *256*, 394. (b) Haddon, R. C. *Aust. J. Chem.* **1975**, *28*, 2333. (c) Haddon, R. C. *Aust. J. Chem.* **1975**, *28*, 2343.

(2) (a) Kinoshita, M.; Turek, P.; Tamura, M.; Nozawa, K.; Shiomi, D.; Nakazawa, Y.; Ishikawa, M.; Takahashi, M.; Awaga, K.; Inabe, T.; Maruyama, Y. *Chem. Lett.* **1991**, 1225. (b) Tamura, M.; Nakazawa, Y.; Shiomi, D.; Nozawa, K.; Hosokoshi, Y.; Ishikawa, M.; Takahashi, M.; Kinoshita, M. *Chem. Phys. Lett.* **1991**, *186*, 401. (c) Chiarelli, R.; Novak, M. N.; Rassat, A.; Tholence, J. L. *Nature* **1993**, *363*, 147. (d) Alberola, A.; Less, R. J.; Pask, C. M.; Rawson, J. M.; Palacio, F.; Oliete, P.; Paulsen, C.; Yamaguchi, A.; Farley, R. D.; Murphy, D. M. *Angew. Chem., Int. Ed.* **2003**, *42*, 4782.

(3) (a) Rawson, J. M.; Alberola, A.; Whalley, A. *J. Mater. Chem.* **2006**, *16*, 2560. (b) Hicks, R. G. *Org. Biomol. Chem.* **2007**, *5*, 1321. (c) Awaga, K.; Tanaka, T.; Shirai, T.; Umezono, Y.; Fujita, W. *C. R. Chimie* **2007**, *10*, 52. (d) Awaga, K.; Tanaka, T.; Shirai, T.; Fujimori, M.; Suzuki, Y.; Yoshikawa, H.; Fujita, W. *Bull. Chem. Soc. Jpn.* **2006**, *79*, 25. (e) Hicks, R. G. *Stable Radicals: Fundamentals and Applied Aspects of Odd-Electron Compounds*; John Wiley & Sons: New York, 2010.

(4) Hubbard, J. *Proc. R. Soc. (London)* **1963**, *A276*, 238.

 10.1021/ja106768z

Chart 1

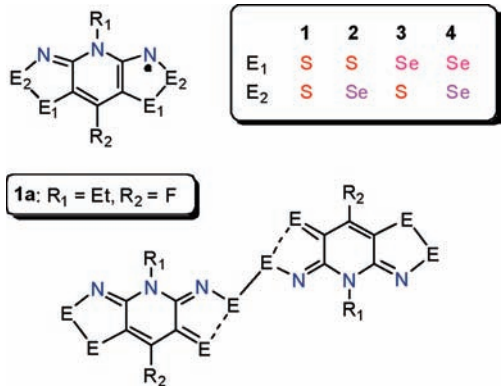

states.[5] Relatively high, albeit not metallic, conductivity can nonetheless be achieved in these strongly correlated systems. Haddon has reported a series of spirophenalenyl radicals,[6] for which $f = {}^1/_4$, and variable-temperature structural and transport property studies[7] on these materials have provided insight into their electronic and magnetic behavior. Activated conductivity has also been observed for resonance-stabilized bisdithiazolyl radicals **1** (Chart 1),[8] which are true $f = {}^1/_2$ systems, and improved conductivity,[9] as well as magnetic ordering, both antiferromagnetic (AFM)[10] and ferromagnetic (FM),[11] has been achieved by the replacement of sulfur by selenium, as in **2**, **3**, and **4**. For the latter systems, the effect on charge and spin transport of the structural changes induced by chemical pressure (molecular modification)[12] and physical pressure[13] has been explored.

In addition to the charge correlation problem, all radical-based materials suffer from a tendency of the radicals to dimerize, either by the formation of localized σ-bonds or through multicenter $\pi-\pi$ bonds.[14] In the case of one-dimensional π-stacked structures,[15] this process can be described in terms of a charge-density-wave (CDW) or Peierls distortion.[16] The consequent pairing of spins, which is facilitated at low temperatures, quenches magnetic interactions and, to the extent that an electronic band model applies, gives rise to the opening of a band gap at the Fermi level. The resulting diamagnetic materials may have a lower conductivity than the parent radical, but there are cases where association actually improves conductivity.[17] There are also a few reports of magnetically bistable radicals, that is, systems which display temperature regimes within which the dimer ($S = 0$) and radical ($S = {}^1/_2$) states can coexist.[17−19] The magnetic hysteresis which is observed with these spin-crossover phase transitions has led to interest in the potential use of bistable radicals in information storage devices.[20] In some cases, hysteresis is apparent in several channels (magnetic, electronic and optical), and these discoveries have fueled the pursuit of multifunctional materials.[21] In addition to the phase changes associated with dimer-to-radical interconversions, there are numerous examples of radicals and radical dimers that crystallize as non-interconvertable polymorphs.[22]

Herein we report the preparation and structural characterization of the bisdithiazolyl radical **1** (R_1 = Et, R_2 = F), hereafter

(5) (a) Mott, N. F. *Proc. Phys. Soc. A* **1949**, *62*, 416. (b) Mott, N. F. *Metal-Insulator Transitions*; Taylor and Francis: London, 1990.
(6) (a) Chi, X.; Itkis, M. E.; Patrick, B. O.; Barclay, T. M.; Reed, R. W.; Oakley, R. T.; Cordes, A. W.; Haddon, R. C. *J. Am. Chem. Soc.* **1999**, *121*, 10395. (b) Pal, S. K.; Itkis, M. E.; Tham, F. S.; Reed, R. W.; Oakley, R. T.; Haddon, R. C. *Science* **2005**, *309*, 281. (c) Mandal, S. K.; Samanta, S.; Itkis, M. E.; Jensen, D. W.; Reed, R. W.; Oakley, R. W.; Tham, F. S.; Donnadieu, B.; Haddon, R. C. *J. Am. Chem. Soc.* **2006**, *128*, 1982. (d) Pal, S. K.; Itkis, M. E.; Tham, F. S.; Reed, R. W.; Oakley, R. T.; Haddon, R. C. *J. Am. Chem. Soc.* **2008**, *130*, 3942.
(7) (a) Haddon, R. C.; Sarkar, A.; Pal, S. K.; Chi, X.; Itkis, M. E.; Tham, F. S. *J. Am. Chem. Soc.* **2008**, *130*, 13683. (b) Bag, P.; Itkis, M. E.; Pal, S. K.; Donnadieu, B.; Tham, F. S.; Park, H.; Schlueter, J. A.; Siegrist, T.; Haddon, R. C. *J. Am. Chem. Soc.* **2010**, *132*, 2684. (c) Huang, J.; Kertesz, M. *J. Am. Chem. Soc.* **2003**, *125*, 13334. (d) Huang, J.; Kertesz, M. *J. Am. Chem. Soc.* **2007**, *129*, 1634. (e) Bohlin, J.; Hansson, A.; Stafstrom, S. *Phys. Rev. B* **2006**, *74*, 155111.
(8) (a) Beer, L.; Brusso, J. L.; Cordes, A. W.; Haddon, R. C.; Itkis, M. E.; Kirschbaum, K.; MacGregor, D. S.; Oakley, R. T.; Pinkerton, A. A.; Reed, R. W. *J. Am. Chem. Soc.* **2002**, *124*, 9498. (b) Beer, L.; Britten, J. F.; Brusso, J. L.; Cordes, A. W.; Haddon, R. C.; Itkis, M. E.; MacGregor, D. S.; Oakley, R. T.; Reed, R. W.; Robertson, C. M. *J. Am. Chem. Soc.* **2003**, *125*, 14394. (c) Leitch, A. A.; Reed, R. W.; Robertson, C. M.; Britten, J. F.; Yu, X.; Secco, R. A.; Oakley, R. T. *J. Am. Chem. Soc.* **2007**, *129*, 7903.
(9) (a) Brusso, J. L.; Derakhshan, S.; Itkis, M. E.; Kleinke, H.; Haddon, R. C.; Oakley, R. T.; Reed, R. W.; Richardson, J. F.; Robertson, C. M.; Thompson, L. K. *Inorg. Chem.* **2006**, *45*, 10958. (b) Brusso, J. L.; Cvrkalj, K.; Leitch, A. A.; Oakley, R. T.; Reed, R. W.; Robertson, C. M. *J. Am. Chem. Soc.* **2006**, *128*, 15080.
(10) Leitch, A. A.; Brusso, J. L.; Cvrkalj, K.; Reed, R. W.; Robertson, C. M.; Dube, P. A.; Oakley, R. T. *Chem. Commun.* **2007**, 3368.
(11) Robertson, C. M.; Leitch, A. A.; Cvrkalj, K.; Reed, R. W.; Myles, D. J. T.; Dube, P. A.; Oakley, R. T. *J. Am. Chem. Soc.* **2008**, *130*, 8414.
(12) (a) Leitch, A. A.; Yu, X.; Winter, S. M.; Secco, R. A.; Dube, P. A.; Oakley, R. T. *J. Am. Chem. Soc.* **2009**, *131*, 7112. (b) Robertson, C. M.; Leitch, A. A.; Cvrkalj, K.; Myles, D. J. T.; Reed, R. W.; Dube, P. A.; Oakley, R. T. *J. Am. Chem. Soc.* **2008**, *130*, 14791.
(13) Mito, M.; Komorida, Y.; Tsuruda, H.; Tse, J. S.; Desgreniers, S.; Ohishi, Y.; Leitch, A. A.; Cvrkalj, K.; Robertson, C. M.; Oakley, R. T. *J. Am. Chem. Soc.* **2009**, *131*, 16012.
(14) Tian, Y.-H.; Huang, J.; Kertesz, M. *Phys. Chem. Chem. Phys.* **2010**, *12*, 5084.
(15) (a) Andrews, M. P.; et al. *J. Am. Chem. Soc.* **1991**, *113*, 3559. (b) Bryan, C. D.; Cordes, A. W.; Goddard, J. D.; Haddon, R. C.; Hicks, R. G.; MacKinnon, C. D.; Mawhinney, R. C.; Oakley, R. T.; Palstra, T. T. M.; Perel, A. S. *J. Am. Chem. Soc.* **1996**, *118*, 330.
(16) Peierls, R. C. *Quantum Theory of Solids*; Oxford University Press: London, 1955; p 108.
(17) Chi, X.; Itkis, M. E.; Kirschbaum, K.; Pinkerton, A. A.; Oakley, R. T.; Cordes, A. W.; Haddon, R. C. *J. Am. Chem. Soc.* **2001**, *123*, 4041.
(18) (a) Fujita, W.; Awaga, K. *Science* **1999**, *286*, 261. (b) Fujita, W.; Awaga, K.; Matsuzaki, H.; Okamoto, H. *Phys. Rev. B* **2002**, *65*, 064434. (c) McManus, G. D.; Rawson, J. M.; Feeder, N.; van Duijn, J.; McInnes, E. J. L.; Novoa, J. J.; Burriel, R.; Palacio, F.; Oliete, P. *J. Mater. Chem.* **2001**, *11*, 1992. (d) Fujita, W.; Awaga, K.; Nakazawa, Y.; Saito, K.; Sorai, M. *Chem. Phys. Lett.* **2002**, *352*, 348. (e) Shultz, D. A.; Fico, R.; Boyle., P. D.; Kampf, J. W. *J. Am. Chem. Soc.* **2001**, *123*, 10403.
(19) (a) Barclay, T. M.; Cordes, A. W.; George, N. A.; Haddon, R. C.; Itkis, M. E.; Mashuta, M. S.; Oakley, R. T.; Patenaude, G. W.; Reed, R. W.; Richardson, J. F.; Zhang, H. *J. Am. Chem. Soc.* **1998**, *120*, 352. (b) Brusso, J. L.; Clements, O. P.; Haddon, R. C.; Itkis, M. E.; Leitch, A. A.; Oakley, R. T.; Reed, R. W.; Richardson, J. F. *J. Am. Chem. Soc.* **2004**, *126*, 8256. (c) Brusso, J. L.; Clements, O. P.; Haddon, R. C.; Itkis, M. E.; Leitch, A. A.; Oakley, R. T.; Reed, R. W.; Richardson, J. F. *J. Am. Chem. Soc.* **2004**, *126*, 14692.
(20) Rota, J.-B.; Le Guennic, B.; Robert, V. *Inorg. Chem.* **2010**, *49*, 1230.
(21) Itkis, M. E.; Chi, X.; Cordes, A. W.; Haddon, R. C. *Science* **2002**, *296*, 1443.
(22) (a) Alberola, A.; Clarke, C. S.; Haynes, D. A.; Pascu, S. I.; Rawson, J. M. *Chem. Commun.* **2005**, 4726. (b) Bond, A. D.; Haynes, D. A.; Pask, C. M.; Rawson, J. M. *J. Chem. Soc., Dalton Trans.* **2002**, 25. (c) Banister, A. J.; Bricklebank, N.; Clegg, W.; Elsegood, M. R. J.; Gregory, C. I.; Lavender, I.; Rawson, J. M.; Tanner, B. K. *J. Chem. Soc., Chem. Commun.* **1995**, 679. (d) Banister, A. J.; Bricklebank, N.; Lavender, I.; Rawson, J. M.; Gregory, C. I.; Tanner, B. K.; Clegg, W.; Elsegood, M. R. J.; Palacio, F. *Angew. Chem., Int. Ed. Engl.* **1996**, *35*, 2533. (e) Leitch, A. A.; McKenzie, C. E.; Oakley, R. T.; Reed, R. W.; Richardson, J. F.; Sawyer, L. D. *Chem. Commun.* **2006**, 1088. (f) Kinoshita, M. *Jpn. J. Appl. Phys.* **1994**, *33*, 5718. (g) Tamura, M.; Hosokoshi, Y.; Shiomi, D.; Kinoshita, M.; Nakazawa, Y.; Ishikawa, M.; Sawa, H.; Kitazawa, T.; Eguchi, A.; Nishio, Y.; Kajita, K. *J. Phys. Soc. Jpn.* **2003**, *72*, 1735. (h) Fatila, E. M.; Jennings, M. C.; Goodreid, J.; Preuss, K. E. *Acta Crystallogr.* **2010**, *C66*, o264.

termed **1a**. This material is dimorphic, crystallizing in one case (α-**1a**) as π-stacked radicals and in the other (β-**1a**) as π-stacked dimers; in the latter structure the dimers consist of pairs of radicals laced together by hypervalent four-center six-electron (4c-6e) S···S−S···S σ-bonds, as shown in Chart 1.[23] Variable-temperature magnetic and conductivity measurements confirm that α-**1a** behaves as a Mott insulator, as do other radicals of this type,[8] with a room-temperature conductivity σ_{RT} near 10^{-6} S cm^{-1}. The lateral mode of dimerization found for β-**1a** is rare for a sulfur-based bisdithiazolyl radical[22e] but has been observed for a number of selenium-containing variants **2**,[24] all of which show a remarkable increase in conductivity with applied pressure. In the case of **2** (R_1 = Me, R_2 = H), the structural and concomitant electronic changes have recently been shown to involve a buckling of the dimeric unit, which causes a sudden closure of the HOMO−LUMO gap, ultimately resulting in metallization of the otherwise semiconducting material.[25] In order to compare the structural and transport properties of hypervalent σ-dimers based on **1** (sulfur) and **2** (selenium), we have performed a detailed analysis of the structure and conductivity of β-**1a** as a function of pressure and temperature. The results of this work have revealed a very different response to elevated pressure and temperature for radicals of type **1** relative to those of type **2**. In contrast to the latter, in which the intermolecular S···Se−Se···S bond remains intact with both increased pressure and temperature, the S···S−S···S bond of β-**1a** opens very readily. At ambient pressure, moreover, the dimer-to-radical interconversion for β-**1a** displays magnetic hysteresis with a narrow window (5 K) of bistability. The solid-state structural and electronic factors underlying the differing behavior of the S···E−E···S σ-dimers (E = S, Se) are discussed in the light of DFT calculations on model systems.

Results

Synthesis. The procedure (Scheme 1) for the preparation of **1a** is based on methods developed for related radicals.[8] Alkylation of 2,4,6-trifluoropyridine (**5**) with ethyl triflate produces *N*-ethyl-2,4,6-trifluoropyridinium triflate (**6**) which, upon treatment with gaseous ammonia, affords the corresponding 2,6-diaminopyridinium triflate (**7**). Double Herz cyclization of the latter with sulfur monochloride in refluxing acetonitrile (MeCN) then furnishes the desired bisdithiazolylium framework in the form of the triflate salt [**1a**][OTf]. Cyclic voltammetry on solutions of this salt in MeCN, with 0.1 M *n*-Bu_4NPF_6 as supporting electrolyte and Pt wire electrodes, confirms the expected series (−1/0, 0/+1, +1/+2) of redox processes, and the half-wave potentials of these couples, which are listed in Table 1, are consistent with those seen for related radicals.[8] Based on these potentials, chemical reduction of [**1a**][OTf] was conveniently effected using decamethylferrocene (DMFc) ($E_{1/2}$(ox) = −0.13 V vs SCE)[26] in MeCN. This afforded **1a** as a black microcrystalline precipitate.

Scheme 1

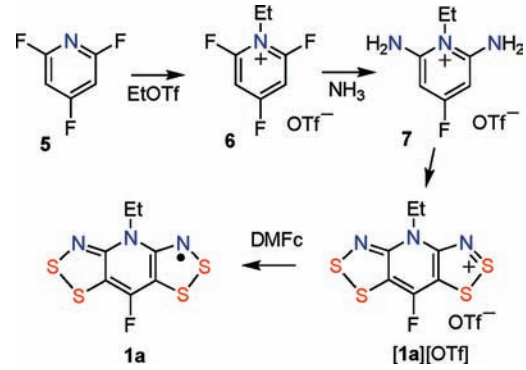

Table 1. Electrochemical Half-Wave Potentials[a] and EPR Parameters for Derivatives of **1**

	R_1, R_2		
	Et, H[b]	Et, Cl[c]	Et, F
$E_{1/2}$(−1/0), V	−0.95[d]	−0.845[d]	−0.822[d]
$E_{1/2}$(0/+1), V	−0.146	−0.018	+0.013
$E_{1/2}$(+1/+2), V	1.292	1.390	1.380
a_N (S), mT	0.318	0.310	0.307
a_N (R_1), mT	0.061	0.060	0.057
a_H (CH_2), mT	<0.02	<0.02	<0.03
a_R (R_2), mT	0.228	0.030[e]	0.637
g-value	2.0082	2.0082	2.0084

[a] In CH_3CN, referenced to SCE. [b] From ref 8b. [c] From ref 8a. [d] Irreversible behavior; E_{pc} value quoted. [e] ^{35}Cl isotope.

Subsequent purification and single-crystal X-ray diffraction analysis of **1a** (vide infra) established the existence of two polymorphs. The material prepared as described above, which can be recrystallized as metallic green needles from hot dichloroethane, constitutes the tetragonal phase α-**1a**. This phase can also be obtained by sublimation of the crude material in vacuo, but dark brown blocks of a second polymorph, subsequently established to be the monoclinic phase β-**1a**, are also produced in the process. Initially, crystals of the two phases were separated manually, but it was later discovered that β-**1a** could be generated almost exclusively by slow sublimation at a pressure of 10^{-4} Torr along a temperature gradient of 60−120 °C. The infrared spectra of the two phases are very different, a feature which provides a simple method for assessing phase purity.[27]

The X-band EPR spectrum obtained by dissolving either phase of **1a** in CH_2Cl_2 at 293 K consists of a seven-line pattern with additional fine structure (Figure 1). This pattern is somewhat different from that observed for the related chloro-substituted derivative **1** (R_1 = Et, R_2 = Cl),[8a] which displays a quintet structure arising from hyperfine coupling to two equivalent dithiazolyl nitrogens ($I(^{14}N) = 1$), the value of a_N (Table 1) being approximately one-half of that observed in monofunctional 1,2,3-dithiazolyls.[28] Spectral simulation for **1a** confirms that a_N remains much the same, but there is

(23) Hypervalent 4c-6e bonds involving combinations of S, Se, and/or Te are well known for systems in which the terminal chalcogens are saturated. See, for example: (a) Nakanishi, W.; Hayashi, S.; Toyota, S. *Chem. Commun.* **1996**, 371. (b) Nakanishi, W.; Hayashi, S.; Arai, T. *Chem. Commun.* **2002**, 2416. (c) Nakanishi, W.; Hayashi, S.; Morinaka, S.; Sasamori, T.; Tokitoh, N. *New J. Chem.* **2008**, *32*, 1881. (d) Sharma, S.; Selvakumar, K.; Singh, V. P.; Zade, S. S.; Singh, H. B. *Phosphorus, Sulfur Silicon Relat. Elem.* **2008**, *183*, 827.

(24) (a) Beer, L.; Brusso, J. L.; Haddon, R. C.; Itkis, M. E.; Kleinke, H.; Leitch, A. A.; Oakley, R. T.; Reed, R. W.; Richardson, J. F.; Secco, R. A.; Yu, X. *J. Am. Chem. Soc.* **2005**, *127*, 1815. (b) Leitch, A. A.; Yu, X.; Robertson, C. M.; Secco, R. A.; Tse, J. S.; Oakley, R. T. *Inorg. Chem.* **2009**, *48*, 9874.

(25) Tse, J. S.; Leitch, A. A.; Yu, X.; Bao, X.; Zhang, S.; Liu, Q.; Jin, C.; Secco, R. A.; Desgreniers, S.; Ohishi, Y.; Oakley., R. T. *J. Am. Chem. Soc.* **2010**, *132*, 4876.

(26) Novriandi, I.; Brown, K. N.; Fleming, D. S.; Gulyas, P. T.; Lay, P. A.; Masters, A. F.; Phillips, L. *J. Phys. Chem.* **1999**, *103*, 2713.

(27) Plots of the infrared spectra of both phases of **1a** are available in the Supporting Information.

(28) (a) Preston, K. F.; Sutcliffe, L. H. *Magn. Reson. Chem.* **1990**, *28*, 189. (b) Kaszynski, P. *J. Phys. Chem. A* **2001**, *105*, 7615.

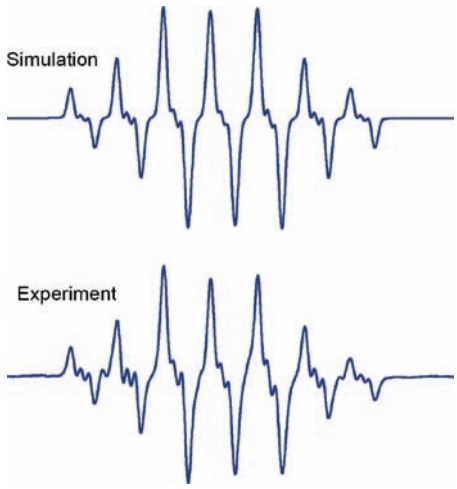

Figure 1. Experimental and simulated EPR spectrum of **1a** in CH_2Cl_2, SW = 3 mT, LW = 0.15 mT, L/G ratio = 0.60.

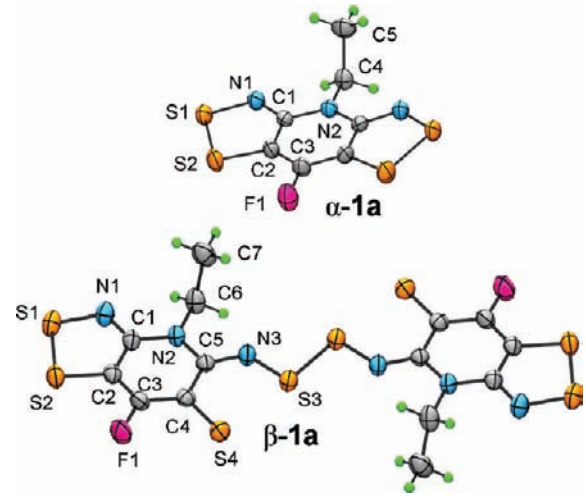

Figure 2. ORTEP drawings (50% probability ellipsoids) of α-**1a** and *β*-**1a** at ambient pressure and temperature, showing atom numbering.

also coupling to fluorine ($I(^{19}F) = {}^1/_2$), in addition to weaker coupling to the pyridine nitrogen and the methylene protons of the *N*-ethyl group.

Crystallography under Ambient Conditions. The crystal structures of both α-**1a** and *β*-**1a** have been determined at ambient temperature and pressure by single-crystal X-ray diffraction. Crystal metrics for the two phases are provided in Table 2, and ORTEP drawings of the molecular building blocks, showing atom numbering schemes, are illustrated in Figure 2.

Crystals of α-**1a** belong to the tetragonal space group $P\bar{4}2_1m$ and are isomorphous with those of **1** (R_1 = Et, R_2 = Cl).[8a] The crystal structure consists of undimerized radicals bisected by mirror planes and locked into pinwheel-like clusters about the $\bar{4}$ centers of the unit cell. Each of the four radicals within the pinwheel provides the basis for a slipped *π*-stack array running along the *z*-direction. The mean interplanar separation *δ* (3.478(1) Å) and the inclination angle *τ* (57.42(1)°) of the mean molecular plane with respect to the stacking axis are similar to those found in **1** (R_1 = Et, R_2 = Cl).[8a] Views of the unit cell of α-**1a** along directions parallel and perpendicular to the stacking axis are shown in Figure 3. While the radicals are not dimerized, that is, there is no pairing of spins into a localized covalent bond, there are numerous intermolecular S···S′ contacts, *d*1 (3.4022(13) Å), *d*2 (3.5311(14) Å), and *d*3 (3.5168(10) Å), within the nominal van der Waals separation for sulfur (3.6 A).[29] As observed in related structures, these contacts generate an extensive lattice-wide network of electronic and magnetic interactions.[11]

Crystals of *β*-**1a** belong to the monoclinic space group $P2_1/c$[30] and consist of interpenetrating, cross-braced slipped *π*-stacks of dimers. At the molecular level these dimers comprise coplanar radicals fused in a centrosymmetric fashion by the hypervalent S4···S3−S3′···S4′ sequence. While the associated S3−S3′ bond length is near that expected for a *σ*-bond, the S3−S4 distance opens to a value intermediate between the sum of the covalent radii[31] and the expected van der Waals contact.[29] Within this supermolecule there is a series of bond length changes relative to those seen in the undisturbed radical found in the tetragonal phase above, the most notable being a shortening of the C5−N3 and C4−S4 distances, all of which are consistent with the closed-shell pseudo-quinoidal valence bond formulation shown in Chart 1.

The packing of the dimers in *β*-**1a** is illustrated in Figure 4A, which shows the ambient-pressure and -temperature unit cell viewed parallel to the *a* axis. Neighboring *π*-stacks along the *z* direction are tilted in opposite directions relative to the *a* axis so as to give the cross-braced pattern shown in Figure 4B. Within this context it is useful to define the slippage angle *τ*,

Table 2. Crystal Data for **1a**

	α-**1a**	*β*-**1a**	*β*-**1a**	*β*-**1a**	*β*-**1a**
pressure, GPa	0	0	0	0.65	0.98
formula	$C_7H_5FN_3S_4$	$C_7H_5FN_3S_4$	$C_7H_5FN_3S_4$	$C_7H_5FN_3S_4$	$C_7H_5FN_3S_4$
M	278.38	278.38	278.38	278.38	278.38
a, Å	15.8542(7)	5.3256(3)	5.2038(4)	5.3225(6)	5.1026(5)
b, Å	15.8542(7)	11.3951(7)	11.6317(4)	11.0910(10)	11.0754(9)
c, Å	4.1273(3)	17.3934(10)	17.7657(9)	17.1492(15)	17.1529(16)
β, deg	90	105.105(2)	105.746(5)	105.095(8)	104.824(8)
V, Å^3	1037.42(10)	1019.06(10)	1034.99(10)	977.42(17)	937.10(15)
ρ_{calcd} (g cm^{-1})	1.782	1.814	1.786	1.891	1.973
space group	$P\bar{4}2_1m$	$P2_1/c^a$	$P2_1/c^a$	$P2_1/c^a$	$P2_1/c^a$
Z	4	4	4	4	4
temp (K)	293(2)	296(2)	393(2)	293(2)	293(2)
μ (mm^{-1})	0.895	0.911	–	–	–
λ (Å)	0.71073	0.71073	1.54056	0.509176	0.509176
data/restr/param	1095/0/76	2444/0/137	–	–	–
solution method	direct methods	direct methods	powder data[b]	powder data[c]	powder data[c]
R, R_w (on F^2)	0.0309, 0.0714	0.0364, 0.0835	0.0797, 0.1421	0.0143, 0.0284	0.0138, 0.0240

[a] The unconventional cell setting ($P2_1/c$ with a large value of *β*) was used so as to allow a direct comparison with related structures. [b] Le Bail refinement. [c] Rietveld refinement.

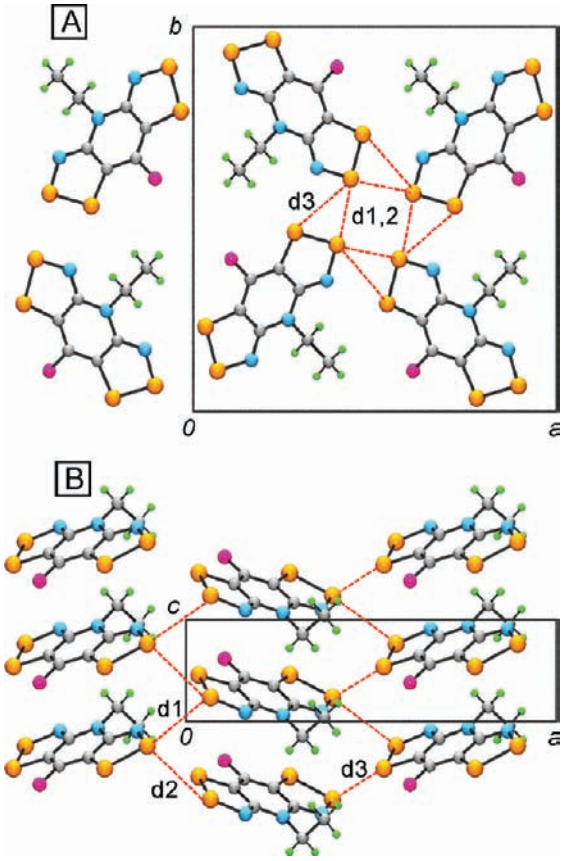

Figure 3. Crystal packing of α-**1a**, viewed along the *z* (A) and *x* (B) directions.

the degree of inclination of the mean molecular plane of the dimer with respect to the stacking axis (the angle at which neighboring dimers along *z* intersect is 2τ). The value of τ, along with the dimer-to-dimer separation along the π-stacks δ, is listed in Table 3. This cross-braced packing arrangement affords a series of close interdimer S---S′ interactions $d1-d3$, the values of which are listed in Table 3. Changes in these parameters, as well as in *q* and *r* (to be defined later), as a function of temperature and pressure are discussed below.

Magnetic Measurements. Magnetic susceptibility (χ) measurements have been performed on the α- and β-phases of **1a** over the temperature range 2−400 K using a SQUID magnetometer operating at a field (*H*) of 1000 Oe. Figure 5 shows the results of preliminary data collected over the range $T = 2-300$ K, presented in the form of plots of χ (corrected for diamagnetic contributions) and χT against *T*. The tetragonal phase α-**1a** behaves as a Curie−Weiss paramagnet, and a fit to the 20−300 K data affords values of $C = 0.348$ emu K mol^{-1} and $\theta = -0.5$ K. The data from the 2−300 K range were also modeled in terms of a Heisenberg chain of AFM coupled $S = {}^1/_2$ radicals, using a fit function based on the molecular-field modified Bonner−Fisher method[32] and the Heisenberg Hamiltonian $H_{ex} = -2\mathbf{J}\{S_1 \cdot S_2\}$.[33] The relatively large and positive (FM) mean-field term $z\mathbf{J}' = +13.3$ cm^{-1} so obtained is consistent with the combined pairwise interstack exchange energies[12] $J_1 = 2.9$ cm^{-1} (with $z = 4$) and $J_2 = 0.6$ cm^{-1} (with $z = 4$) estimated using broken-symmetry DFT methods.[34,35] Likewise, the AFM exchange energy $\mathbf{J} = -9.6$ cm^{-1} extracted from the 1D chain

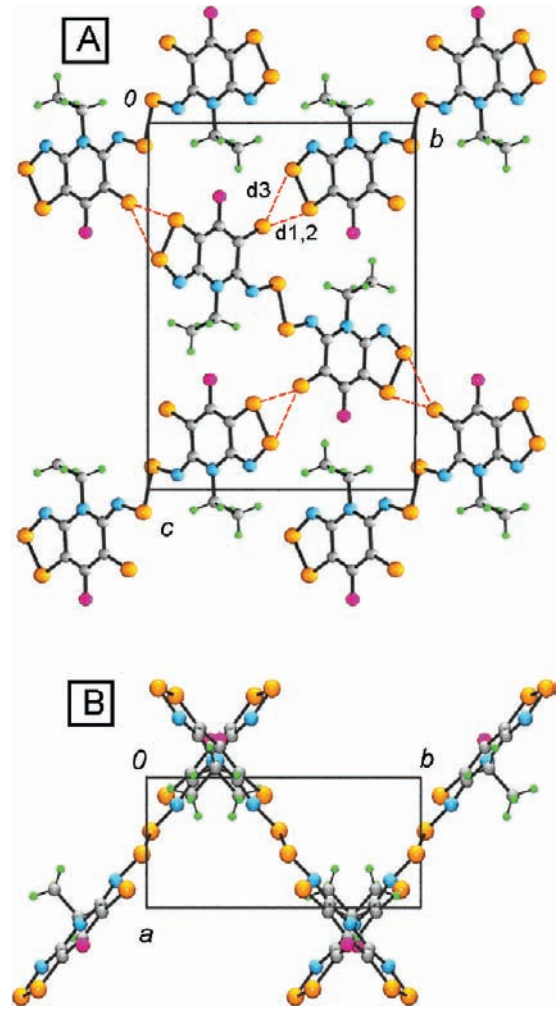

Figure 4. Crystal packing of β-**1a** at ambient *T* and *P*, viewed along the *x* (A) and *z* (B) directions.

Table 3. Structural Parameters for β-**1a** as a Function of Temperature and Pressure

temp (K)	296(2)	393(2)	293(2)	293(2)
pressure (GPa)	0	0	0.65	0.98
S3−S3′ (Å)	2.1687(13)	−	2.248	−
S3−S4 (Å)	2.794	2.167	2.739	2.185
S2···S4′, *d*1 (Å)	3.321	3.493	3.293	3.133
S2···S4′, *d*2 (Å)	3.550	3.507	3.431	3.302
S1···S4′, *d*3 (Å)	3.375	3.835	3.311	3.351
S3···N4′, *d*4 (Å)	−	2.981	−	3.048
τ (deg)	42.49(1)	42.58	40.47	41.19
δ (Å)	3.584(1)	3.519	3.449	3.358
r (Å)	2.169	2.977	2.246	3.036
q (Å)	−0.046	1.526	0.093	1.946

(29) (a) Bondi, A. *J. Phys. Chem.* **1964**, *68*, 441. (b) Dance, I. *New J. Chem.* **2003**, *27*, 22.
(30) The $P2_1/c$ space group setting was used (rather than the alternate $P2_1/n$) for β-**1a** to allow for a direct comparison of this structure with the dimers found for **2** (R_1 = Me; R_2 = H, Me, F) which had been solved in $P2_1/c$ (refs 24 and 25).
(31) Chen, C. M.; Dojahn, J. G.; Wentworth, W. E. *J. Phys. Chem. A* **1997**, *101*, 3088.
(32) Bonner, J. C.; Fisher, M. E. *Phys. Rev. A* **1964**, *135*, 640.
(33) Details of the Bonner−Fisher fit for the magnetic data of α-**1a** are provided in the Supporting Information.
(34) (a) Noodleman, L.; Norman, J. G. *J. Chem. Phys.* **1979**, *70*, 4903. (b) Noodleman, L. *J. Chem. Phys.* **1981**, *74*, 5737. (c) Deumal, M.; Robb, M. A.; Novoa, J. J. *Prog. Theor. Chem. Phys.* **2007**, *16*, 271.

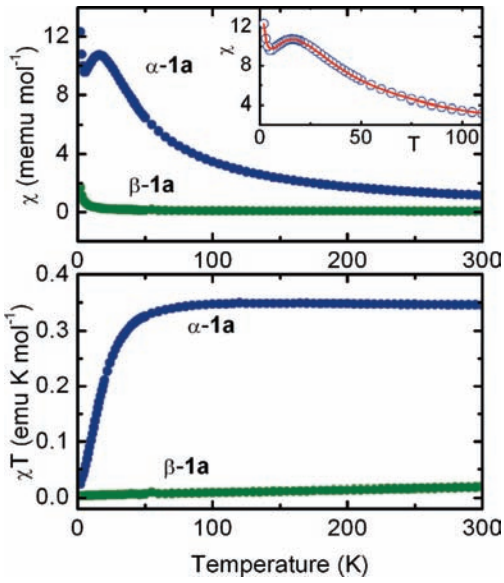

Figure 5. Plots of χ (above) and χT (below) versus T for α-**1a** and β-**1a** from $T = 2$ to 300 K. The inset shows the fit of χ versus T for α-**1a** to a 1D chain of AFM coupled $S = {}^1/_2$ radicals.

model is in accord with that calculated for the intrastack[12] exchange interaction, $J_\pi = -14.1$ cm^{-1}.

As expected from the presence of a covalent bond between the two radicals in the dimeric unit in β-**1a**, the near-baseline plot (Figure 5) of χ versus T indicates that the material is essentially diamagnetic over the temperature range 2−300 K; the small Curie "tail" observed at low temperatures may be ascribed to radical defects. The related plot of χT against temperature indicates a very slow increase in χT to a value of 0.019 emu K mol^{-1} at 300 K, which corresponds to a defect concentration of about 5%. This result is in keeping with the behavior of related dimers.[24] However, the fact that β-**1a** can be vaporized under relatively mild conditions (120 °C/10^{-4} Torr) led us to consider whether the dimer might actually dissociate in the solid state prior to vaporization. To explore this possibility, we extended the temperature range for the measurement of the magnetic susceptibility to $T = 400$ K. The results, illustrated in Figure 6 in the form of a χT versus T plot from $T = 300$ to 400 K, reveal a sharp rise in χT at $T^{\uparrow} = 380$ K to a plateau near 0.33 emu K mol^{-1}, a value close to that expected (0.375 emu K mol^{-1}) for a fully dissociated radical with $S = {}^1/_2$ and a nominal g-value of 2. Moreover, upon cooling the sample, the χT value reverts to its original near-diamagnetic value, but the changeover occurs at a slightly lower temperature ($T^{\downarrow} = 375$ K) than that found during the heating process. Collectively these changes represent the signature of a hysteretic dimer-to-radical phase change, with a region of bistability of about 5 degrees Kelvin.

High-Temperature Crystallography. In order to investigate the structural changes associated with the phase transition observed in the magnetic measurements, we performed a high-temperature ($T = 393$ K) structural analysis of β-**1a** using powder X-ray diffraction methods. The powder pattern so obtained (Figure 7) was indexed and solved with DASH using a model geometry for the molecule taken from a UB3LYP/6-311G(d,p) calculation. During the initial refinement in DASH a rigid-body constraint was maintained, but the sulfur positions were later released to optimize within the plane of the molecule. Given the high thermal motion and consequent low resolution of the diffraction pattern, the final structural refinement was performed using Le Bail methods. Crystal data and relevant metrics are compiled in Tables 2 and 3, and a unit cell drawing is illustrated in Figure 8. In accord with the magnetic measurements, the high-temperature form of β-**1a** consists of undimerized radicals. The intermolecular S3−S3′ bond present at ambient temperature is replaced by weak four-center S3···N4′ interactions (*d*3), a common feature of the packing of thiazyl heterocycles (vide infra), and the transannular hypervalent S3−S4 contact closes to a value comparable to that of S1−S2, that is, a normal covalent S−S distance. In addition, there are also long-range intermolecular S2···S4′ contacts (Table 3) that lace together molecules up and down the stacking direction.

(35) Details of the UB3LYP/6-311G(d,p) calculations of the pairwise exchange energy calculations for β-**1a** are provided in the Supporting Information. The definitions for J_1, J_2, and J_π are taken from ref 12b.

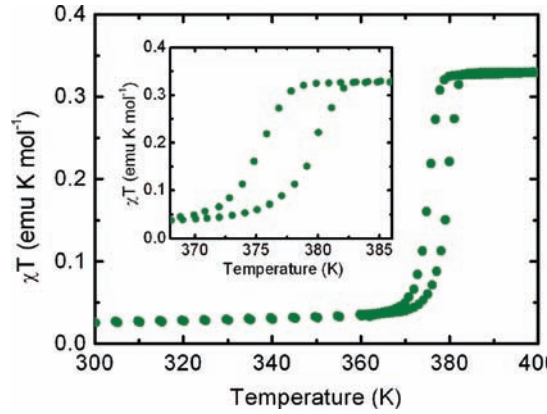

Figure 6. Plot of χT versus T for β-**1a** from $T = 300$ to 400 K, showing hysteretic phase transition.

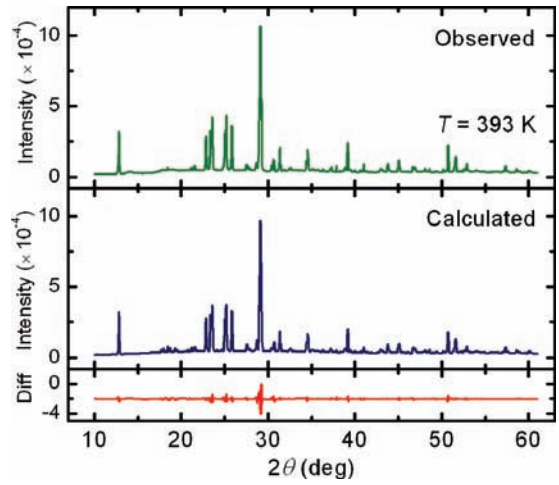

Figure 7. Observed and calculated powder X-ray diffraction pattern for β-**1a** at 393 K ($\lambda = 1.5406$ Å).

Conductivity Measurements. Pressure-dependent conductivity measurements over the temperature range $T = 300-400$ K have been performed on both phases of **1a**, using a cubic anvil press. The initial purpose of this exercise was to extract thermal activation energies for the conductivity of the two structures as a function of pressure, but it soon became apparent that the behavior of the two phases under pressure was quite different. To demonstrate this, we show in Figure 9 plots of the pressure dependence of the conductivity of both phases at ambient

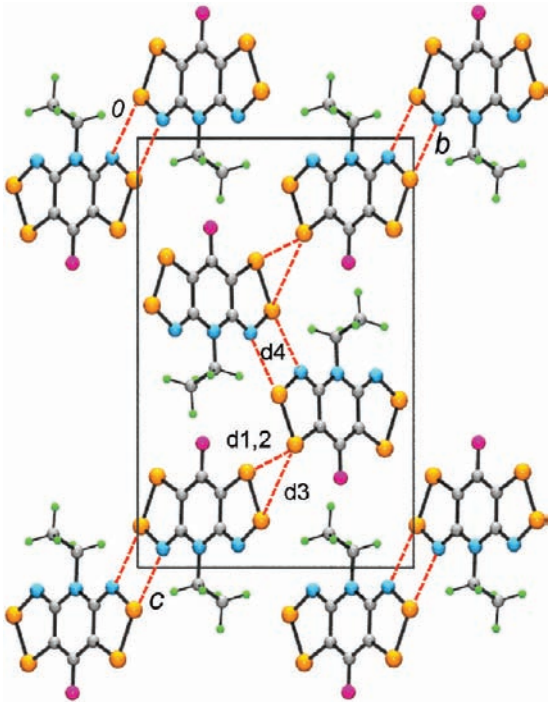

Figure 8. Crystal packing of β-**1a** at $T = 393$ K, viewed along the x direction.

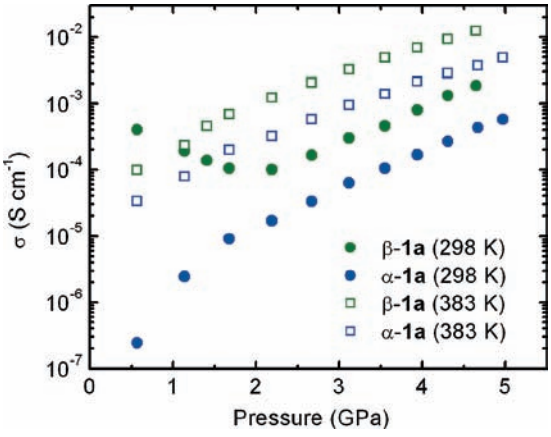

Figure 9. Conductivity of α- and β-**1a** as function of pressure.

temperature ($T = 298$ K) and also at $T = 383$ K, that is, just above the transition temperature for the dimer-to-radical conversion of the monoclinic β-phase. For both phases the data collected at 383 K reveal a smooth and steady increase in conductivity of about 2 orders of magnitude over the pressure range 0.5−5 GPa, as would be expected, given that, at this temperature, both structures consist of slipped π-stacks of radicals. The α-phase is less conductive than the β-phase, a feature which provides a simple and elegant illustration of how changes in packing patterns based on exactly the same molecular building block can result in significant differences in solid-state electronic structure and hence charge transport properties.

At ambient temperature (298 K), the σ versus P plot for α-**1a** shows the same trend as that observed at $T = 383$ K, although the increase in conductivity is somewhat larger, now spanning over 3 orders of magnitude. In addition, and as expected for a thermally activated process, the conductivity at 298 K at a given pressure is lower than that observed at 383 K. Values of the thermal activation energy E_{act} extracted from a series of $\sigma(P,T)$ measurements over the ranges $T = 298-383$ K and $P = 0.5-5.0$ GPa are plotted in Figure 10. The results show a pressure-driven decrease in E_{act} from near 0.50 eV at 0.5 GPa to near 0.30 eV at 5.0 GPa, a variation which parallels the trends seen for other slipped π-stack radicals of type **1**.[36]

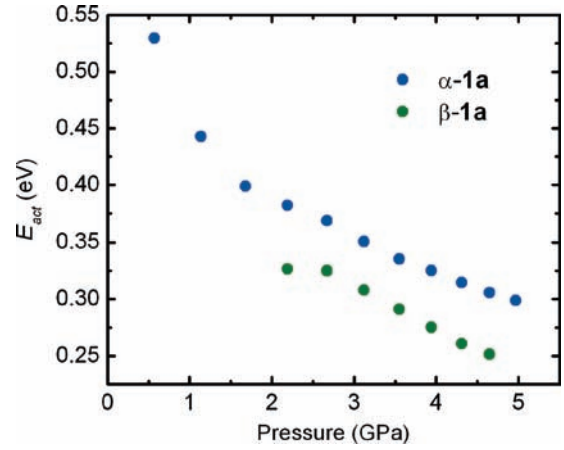

Figure 10. Activation energy for conductivity E_{act} of α- and β-**1a** as function of pressure.

The pressure dependence of $\sigma(P)$ for β-**1a** at 298 K is more complex than that observed for α-**1a** at the same temperature, and indeed that displayed by β-**1a** itself at 383 K. Instead of a steady rise in conductivity with increasing pressure, the value of σ(298 K) actually decreases from 4×10^{-4} S cm^{-1} at 0.5 GPa to 1×10^{-4} S cm^{-1} at 1.5 GPa. At pressures beyond 2.0 GPa the trend reverses, and the value of σ(298 K) increases steadily along a path which parallels that observed for α-**1a**. These changes, along with the fact that σ(298 K) for β-**1a** at 0.5 GPa is over an order of magnitude greater than σ(383 K) at the same pressure, can be interpreted in terms of the fact that, in its dimeric form, β-**1a** behaves as a small-band-gap semiconductor. With increasing temperature or pressure, the dimer eventually dissociates to afford a Mott insulating radical structure, the conductivity of which is lower (by an order of magnitude) than that of the diamagnetic dimer.[37] Values of the thermal activation energy E_{act} above 2 GPa, extracted from the variation in conductivity with temperature and plotted in Figure 10 as a function of pressure, are lower than those found for α-**1a**, but the rate of decrease in E_{act} with pressure of the two phases is qualitatively similar.

High-Pressure Crystallography. In order to investigate the structural nature of the phase change observed in the high-pressure conductivity measurements on β-**1a**, a series of powder diffraction data sets on β-**1a** were collected at room temperature as a function of increasing pressure, using synchrotron radiation ($\lambda = 0.509176$ Å) and diamond anvil cell techniques. Inspection of changes in the powder patterns and the consequent variations in the unit cell volume, obtained from DASH (Figure 11) over the pressure range 0−1.2 GPa, suggested the occurrence of a first-order phase transition[38] between 0.6 and 0.8 GPa.[39] Accordingly, two data sets collected at 0.65 and 0.98 GPa, that is, just below and above and the phase transition, were solved

(36) Beer, L.; Brusso, J. L.; Haddon, R. C.; Itkis, M. E.; Oakley, R. T.; Reed, R. W.; Richardson, J. F.; Secco, R. A.; Yu, X. *Chem. Commun.* **2005**, 5745.

(37) The rather sluggish dimer-to-radical phase change with pressure, indicated by the slow change in conductivity over the pressure range 0.5−2.0 GPa, probably reflects a less than perfectly isotropic pressurization of the sample in the cubic anvil press.

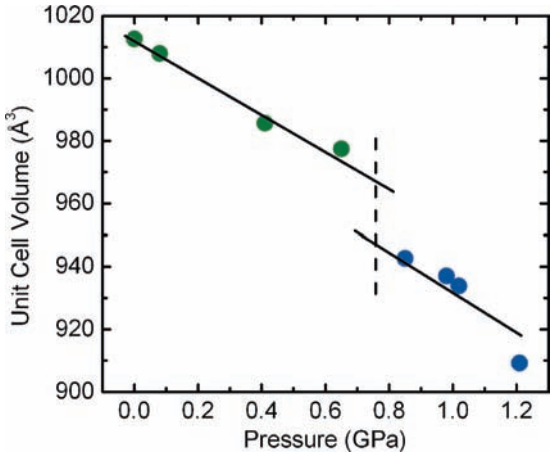

Figure 11. Change in unit cell volume of β-**1a** as a function of pressure.

starting from a model radical **1a** derived from a fully optimized UB3LYP/6-311G(d,p) calculation. During the initial Rietveld refinement, performed using DASH, a rigid-body constraint was maintained, but the sulfur positions were later released to optimize within the plane of the molecule. The final Rietveld refinement, with fixed atomic positions and isotropic thermal parameters, was performed using GSAS. The experimental and final calculated powder patterns for the two data sets are shown in Figure 12. Final unit cell and refinement parameters are listed in Table 2.

The crystallographic results confirm a phase transition between 0.65 and 0.98 GPa and establish that, at a molecular level, the structural changes are the same as those induced by heating, that is, a spin crossover from a 4c-6e hypervalent σ-dimer to a π-radical pair linked by weak intermolecular S···N′ contacts. These changes are illustrated in Figure 13 by means of comparative plots of the disulfide core at 0.65 GPa and the π-radical pair at 0.95 GPa. Concomitant with these changes, there is a general compression in the intermolecular S···S′ contacts, values of which are summarized in Table 3.

Discussion

From a structural perspective, the bisdithiazolyl radical **1a** is interesting for several reasons. First, it is dimorphic, crystallizing in two distinct morphologies, the α-phase consisting of π-stacked radicals and the β-phase comprising π-stacked hypervalent 4c-6e σ-dimers. While the tetragonal packing motif of the α-phase has been observed before,[8] indeed it is the structure type displayed by the ferromagnetic radicals **2** and **4** (R_1 = Et, R_2 = Cl),[11] the hypervalent σ-dimer motif is uncommon for sulfur-based radicals **1**.[22g,40] The second feature of note is the response of the β-phase to increases in temperature and pressure, both of which cause the σ-dimer to open into a pair of π-radicals. This phase transition has been identified crystallographically but is also manifest through changes in the magnetic and

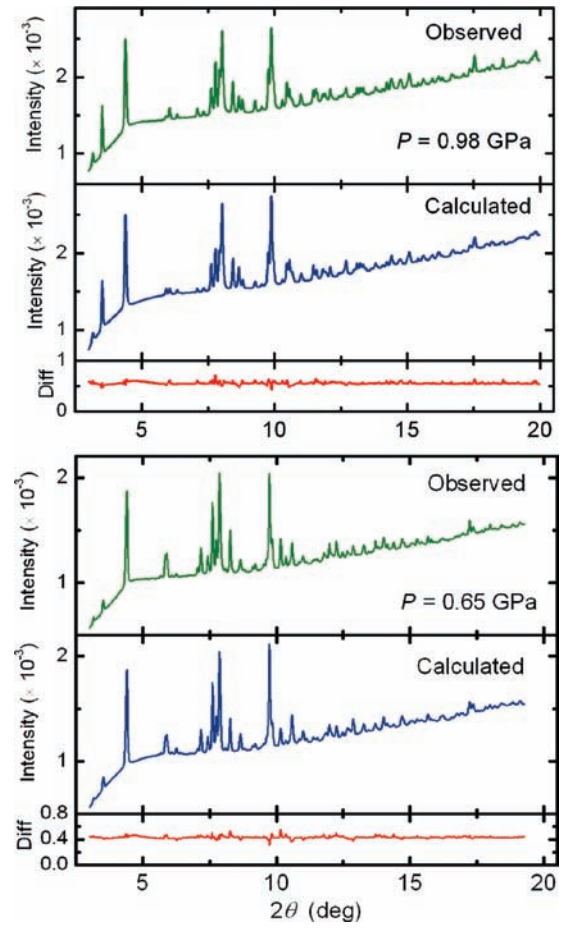

Figure 12. Observed and calculated powder X-ray diffraction pattern for β-**1a** at 0.65 and 0.98 GPa (λ = 0.509176 Å).

conductive properties of the material. In the magnetic channel the spin crossover from the σ-dimer ($S = 0$) to the π-radical ($S = {}^1/_2$) is sharp and slightly hysteretic, displaying a range of bistability of about 5 degrees Kelvin. At the same time the conversion of the closed-shell σ-dimer, a small-band-gap semiconductor, to an open-shell π-radical, an $f = {}^1/_2$ Mott insulator, gives rise to a decrease in conductivity.

The ability to alter both the structure and transport properties of β-**1a** through changes in temperature and pressure makes this type of system of potential value in the development of new electronic and magnetoelectronic materials.[21,41] There are several questions, however, that need to be addressed before such an endeavor might be pursued. Can we understand, for example, the origin of the magnetic hysteresis associated with the dimer-to-radical interchange? Likewise, is it possible to rationalize the structural response to pressure of β-**1a** with that of the hypervalent σ-dimer based on the related Se-centered radical **2** (R_1 = Me, R_2 = H)? While the latter crystallizes in the same space group and with the same packing pattern as β-**1a**, it does not dissociate under pressure, to form a Mott insulator, but instead undergoes a semiconductor-to-metal phase

(38) We note that the PV work calculated from the volume change (~20 Å^3) at the phase transition is on the same order of magnitude as the estimated thermal activation energy.

(39) The higher pressure observed for the phase transition in the conductivity experiments reflects differences in the hydrostaticity of the two presses. At low pressures using silicone oil as the pressure-transmitting medium (assuming no penetration of oil into the sample), the diamond anvil cell is more hydrostatic than the solid medium high-pressure cubic anvil press.

(40) Beer, L.; Reed, R. W.; Robertson, C. M.; Oakley, R. T.; Tham, F. S.; Haddon, R. C. *Org. Lett.* **2008**, *10*, 3121.

(41) (a) Wolf, S. A.; Awschalom, D. D.; Buhrman, R. A.; Daughton, J. M.; von Molnár, S.; Roukes, M. L.; Chtchelkanova, A. Y.; Trege, B. D. M. *Science* **2001**, *294*, 1488. (b) Prinz, G. A. *Science* **1998**, *282*, 1660. (c) Naber, W. J. M.; Faez, S.; van der Wiel, W. G. *J. Phys. D: Appl. Phys.* **2007**, *40*, R205.

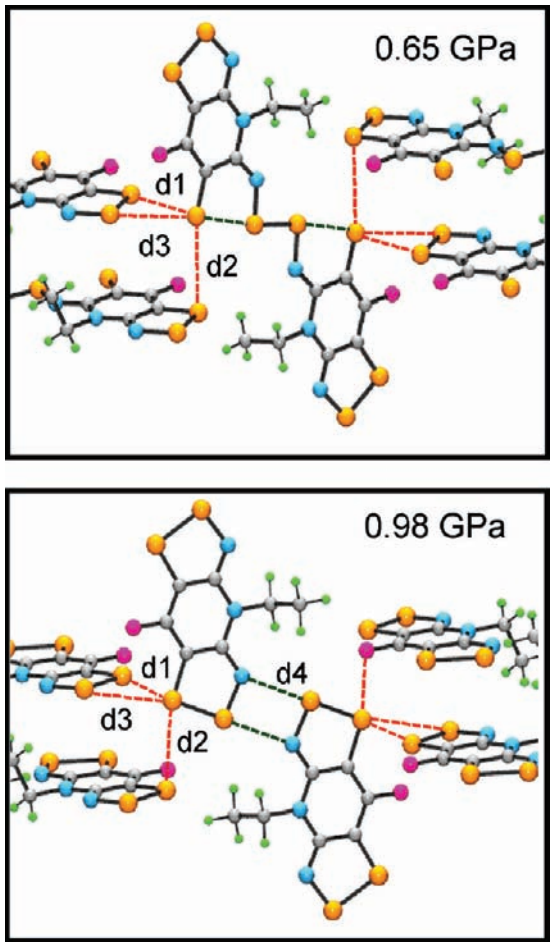

Figure 13. Transformation of β-**1a** from a 4c-6e σ-dimer at 0.65 GPa to a π-radical pair at 0.98 GPa.

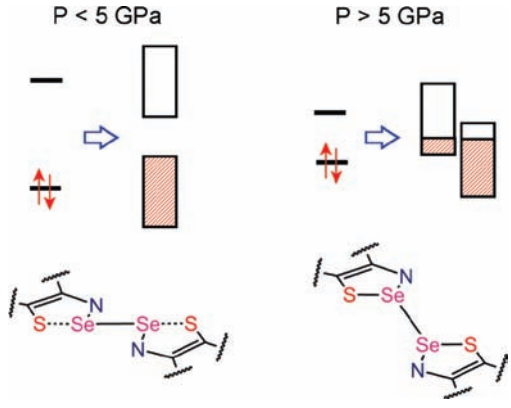

Figure 14. Electronic changes associated with buckling of σ-dimer **2** (R_1 = Me, R_2 = H) under pressure.

transition near 5 GPa.[42] Crystallographic analysis revealed not a dimer-to-radical switchover, as observed here, but a distortion in which the *planar* σ-dimer buckles to form a strained π-dimer, as illustrated in Figure 14.[25] This deformation allows for an overall compression of the molecular framework and also gives rise to a sharp decrease in the HOMO−LUMO gap, a process which, when coupled with the expected effects of compression

(42) High-temperature magnetic susceptibility measurements on **2** (R_1 = Me, R_2 = H) have confirmed that this material does not dissociate below 400 K.

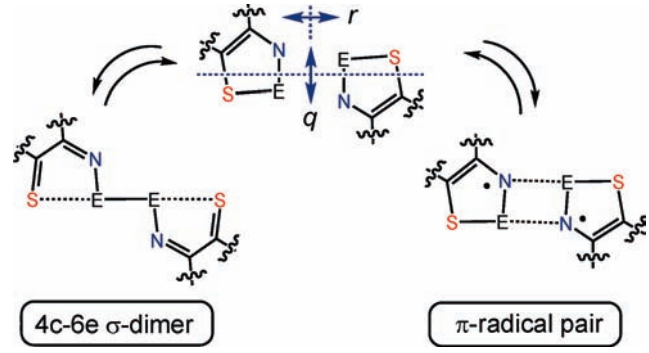

Figure 15. Evolution of a 4c-6e σ-dimers **1** and **2** (R_1 = R_2 = H; E =S, Se) into a pair of π-radicals.

on band broadening, leads to a closure of the valence-to-conduction band gap and the formation of a weakly metallic state. In our analysis of the buckling process of **2a**, we estimated (for E = Se) an energy barrier of about 20 kcal mol^{-1} for the conversion of the σ-dimer to a distorted π-dimer. Using the same model and theoretical method, we find an almost identical barrier for E = S, and from this result we conclude that the dissociation of β-**1a** to produce a pair of π-radicals must be energetically a much more facile process. If, however, that is the case, why do dimers based on **2** (with E = Se) not also slide apart under pressure to afford radicals?

To explore these issues we have examined, at the (U)B3LYP/6-31G(d,p) level, the total energy changes associated with the transformation of S···S−S···S and S···Se−Se···S σ-dimers into pairs of π-radicals, using models of **1** and **2** with R_1 = R_2 = H, each optimized within the constraints of C_{2h} symmetry. The reaction path for this idealized process, illustrated in Figure 15, can be conveniently expressed in terms of (i) the separation (r) between the E−N bonds of the two radicals and (ii) the relative slippage coordinate (q) of the two radicals, defined such that q = 0 when the hypervalent S···E−E···S sequence is collinear. Observed values for these parameters in the crystal structure of β-**1a** are provided in Table 3.

Inspection of the idealized molecular orbital manifolds (Figure 16) of these two systems, each in C_{2h} symmetry, reveals that interconversion of the two structures requires a configurational crossover. There are three occupied σ-type orbitals (two a_g and one b_u) associated with the hypervalent 4c-6e S···E−E···S unit, whereas in the radicals there are only two occupied σ-type orbitals (a_g and b_u), essentially one for each E−E bond. The remaining two σ-electrons from the dimer are transferred to the π-SOMOs (b_g and a_u) of the radicals, high-spin occupation of which gives rise to a ^3B_u state. The computational challenge lies in estimating the relative energies of the two states, the closed-shell σ-dimer and the ^3B_u radical pair, as a function of r and q parameters defined in Figure 15. In the case of the σ-dimer, this is a relatively straightforward task. For small q-values, that is, relatively minor distortions of the hypervalent S···E−E···S sequence away from collinearity, the resulting state is bound, as a result of which the value of r could be included in the geometry optimization. By contrast, the ^3B_u radical pair state is unbound, and optimized total energy calculations as a function of q require that the value of r be fixed. In the case of **1** (R_1 = R_2 = H), we set r = 3.0 Å, this value being close to that observed in the high-pressure and high-temperature structures of β-**1a** itself (Table 3). For **2** (R_1 = R_2 = H), a slightly smaller value (r = 2.8 Å) was used, as in most

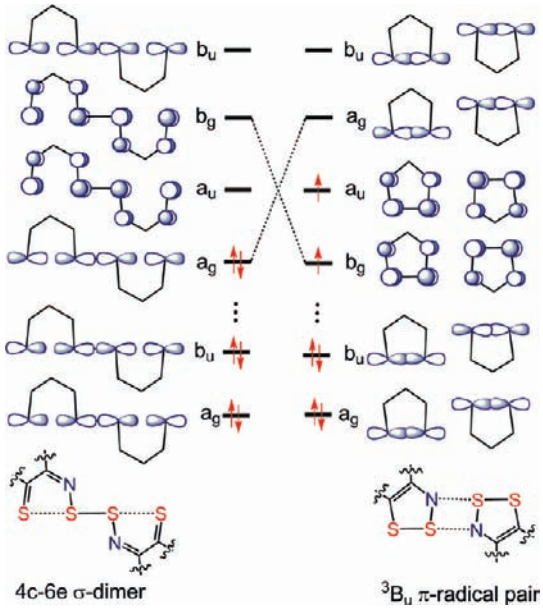

Figure 16. Frontier molecular orbitals of 4c-6e σ-dimer (left) and triplet (^3B_u) π-radical pair (right).

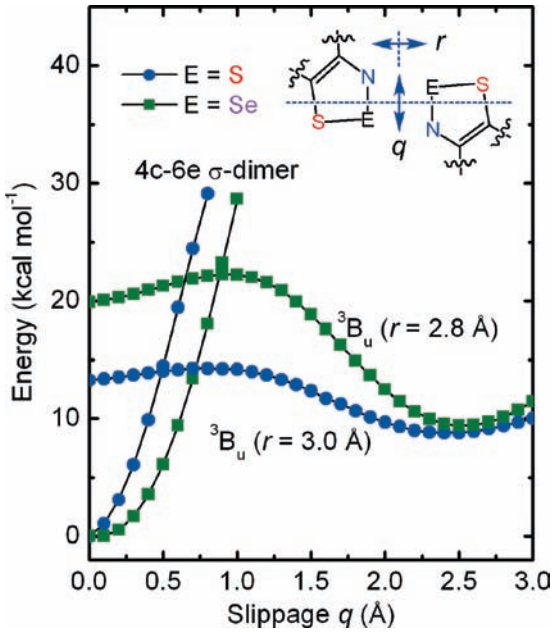

Figure 17. (U)B3LYP/6-31G(d,p) total electronic energy of model 4c-6e σ-dimers and triplet (^3B_u) π-radical pairs of **1** and **2** ($R_1 = R_2 = H$).

structures possessing four-center $(Se\cdots N')_2$ interactions[24,43] the intermolecular "secondary bonds" are stronger, and hence shorter, than the corresponding $(S\cdots N')_2$ interactions in the sulfur compounds.[44]

The numerical results are summarized in Figure 17, in the form of plots of the total energy of the σ-dimer states for **1** and **2** ($R_1 = R_2 = H$), fully optimized at values of the slippage coordinate q from 0 to 1 Å, and the ^3B_u states for the corresponding radical pairs, each constrained to the preset separation parameter r noted above but otherwise fully optimized. While correlation differences between the triplet and singlet states preclude a quantitative analysis, the results allow assessment of the *relative* ease of conversion of a 4c-6e σ-dimer into a pair of radicals as a function of the slippage parameter q. In this regard we note two features. The first is that the potential surface for distortion of the σ-dimers is much steeper for E = S than for E = Se. This may reflect a weaker long-range overlap between adjacent sulfur 3p-orbitals in comparison to selenium 4p-orbitals, so that the Se-based dimer is more flexible. The second factor that must be taken into account is the energy surface of the ^3B_u state, onto which the singlet σ-dimer surface must cross. At small values of q, this surface is much higher lying for E = Se than for E = S, while at larger values of q, the energy minimum for E = Se becomes more pronounced than for E = S, indicative of the stronger secondary bonding interactions expected at this geometry. Taken together, these two effects give rise to a situation in which the crossover from the energy surface of the σ-dimer singlet for **2** (E = Se) to the corresponding ^3B_u radical pair requires a much greater motion along the distortion coordinate q in comparison to that for **1** (E = S). As a result, the barrier for the dimer-to-radical conversion for **2** (22 kcal mol^{-1}) is significantly greater than that for **1** (14 kcal mol^{-1}). Likewise the reverse process, the radical-to-dimer switch, is also associated with a higher barrier for **2** (13 kcal mol^{-1}) than for **1** (5 kcal mol^{-1}).

While the relatively low estimated barriers for the interconversion of the σ-dimer and radical pair of **1** ($R_1 = R_2 = H$) are broadly consistent with the ease of thermal and pressure-induced dissociation of β-**1a**, the higher values calculated for the corresponding Se-based system do not, by themselves, provide a definitive reason as to why solid-state dissociation of dimers based on **2** does not occur. The barrier for dissociation (22 kcal mol^{-1}) is, in fact, comparable to that estimated (20 kcal mol^{-1}) for the buckling process shown in Figure 14, and yet there is no evidence for any competition between the two modes of deformation. To address this issue, we need to go beyond the idealized gas-phase models used so far and examine the supramolecular architecture of β-**1a** and **2** (R_1 = Me, $R_2 = H$).

To this end, we illustrate in Figures 18 and 19 the ribbon-like arrays of σ-dimers in β-**1a** and **2** (R_1 = Me, $R_2 = H$), within which adjacent dimers are bridged by four-center secondary bonding $(E\cdots N')_2$ contacts (E = S, Se). For convenience and consistency with the previous analysis, we define the geometrical extent of these interactions in terms of the parameters r' and q'. The large value of r' found for the $(S\cdots N')_2$ contacts in β-**1a** suggests a very weak intermolecular interaction, with neighboring dimers essentially disconnected and free to move independently. As a result, the conversion of the dimers into radicals, a process which leads to compression of the overall length $(S1\cdots S1')$ of the supermolecule from 16.060 to 15.385 Å, is not compromised by the secondary bonding interactions. Consistently, the interdimer contact r' lengthens slightly (from 3.603 to 3.705 Å) and q' decreases substantially (from 2.624 to 2.160 Å) as neighboring dimers slide apart. In essence, the energetics of the process can be reasonably described, to a first approximation, in terms of the gas-phase molecular model described above.

By contrast, in the Se-based dimer **2** (R_1 = Me, $R_2 = H$), the interdimer secondary bonding interactions are much stronger ($r = 2.839$ Å) at ambient pressure and have the effect of locking together adjacent dimers along the ribbon. As a result, lateral motion required to convert a dimer into a pair of radicals is

(43) Dutton, J. L.; Tindale, J. J.; Jennings, M. C.; Ragogna, P. J. *Chem. Commun.* **2006**, 2474.

(44) (a) Cozzolino, A. F.; Vargas-Baca, I.; Mansour, S.; Mahmoudkhani, A. H. *J. Am. Chem. Soc.* **2005**, *127*, 3184. (b) Cozzolino, A. F.; Vargas-Baca, I. *J. Organomet. Chem.* **2007**, *692*, 2657.

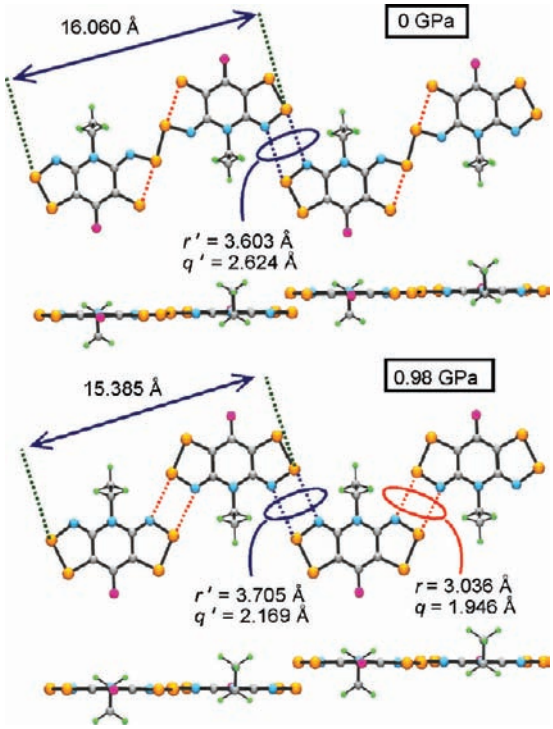

Figure 18. Supramolecular distances r' and q' along molecular ribbons of β-**1a** at 0 and 0.98 GPa.

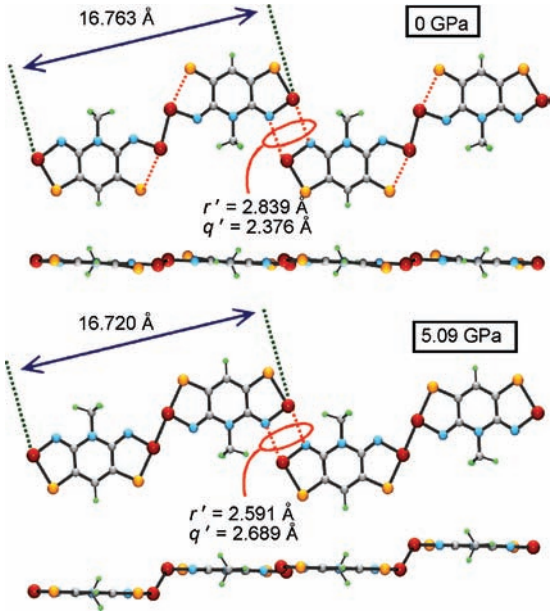

Figure 19. Supramolecular distances r' and q' along molecular ribbons of **2** (R_1 = Me, R_2 = H) at 0 and 5.09 GPa.

energetically unfavorable. Even though the gas-phase estimates suggest that opening of the Se-based σ-dimer is energetically comparable to buckling, it is the latter motion, which preserves the strong interdimer $(Se\cdots N')_2$ supramolecular synthons,[45] which is actually observed. Indeed, under a pressure of 5 GPa, the value of r' contracts to 2.591 Å, in accord with this interpretation.

Summary

In the solid state, most bisdithiazolyls **1** studied to date crystallize as discrete radicals rather than dimers, and adopt a single-crystalline phase. Compound **1a**, the focus of this report, breaks with precedent in several ways. It is dimorphic, the α-phase crystallizing as π-stacked radicals in the tetragonal space group $P\bar{4}2_1m$, while the β-phase consists of π-stacked dimers in which two radicals are bound by a hypervalent 4c-6e $S\cdots S-S\cdots S$ linkage. Such dimeric structures have been previously observed for selenium-based radicals **2**, but the responses of the molecular and bulk properties of the $S\cdots E-E\cdots S$ linked materials (E = S, Se) to pressure and temperature are quite different. In contrast to the behavior of related Se−Se-based σ-dimers, which retain their dimeric structure under pressure, the S−S-based dimer β-**1a** readily dissociates under pressure or with heating, and the associated phase transition can be observed through changes in both conductivity and magnetic susceptibility.

The difference in the behavior of the two systems in response to increases in temperature and pressure arises from a combination of molecular and lattice-based effects. The Se-based radicals **2** are bound more strongly, not only in terms of the hypervalent linkage but also in terms of the supramolecular four-center $(Se\cdots N')_2$ secondary bonding interactions, which lock the dimers into rigid chains. Thermal energy (<400 K) is insufficient to induce dissociation, while applied pressure leads to buckling of the dimers with retention of the secondary bonding linkages. By contrast, the supramolecular $(S\cdots N')_2$ interactions in the S-based dimer β-**1a** are weak, and changes in the packing of the molecules and the lattice parameters in the course of the phase transition are minimal. As a result, cooperative structural effects are likely to be small, and the hysteresis observed from the spin crossover may stem largely from the fact that dissociation of the dimers, and reassociation of the radicals, is symmetry forbidden, a feature not observed for the conventional modes of dimerization open to thiazyl radicals.

It remains to be seen whether the magnetic bistability found for β-**1a** is a general phenomenon for these hypervalent $S\cdots S-S\cdots S$ σ-dimers, or whether such systems will find device applications comparable to those of transition-metal-based spin-crossover compounds.[46] In the meantime, we are pursuing ways to enhance the width of the bistable regime of these systems by molecular modification.

Experimental Section

General Methods and Procedures. The reagents 2,4,6-trifluoropyridine (**5**), ethyl trifluoromethanesulfonate (ethyl triflate, EtOTf), anhydrous ammonia, sulfur monochloride, and decamethylferrocene (DMFc) were obtained commercially. All were used as received except for DMFc, which was sublimed in vacuo before use. The solvents acetonitrile (MeCN), dichloroethane (DCE), dichloromethane (DCM), carbon disulfide, and diethyl ether were of at least reagent grade. MeCN was dried by distillation from P_2O_5 and/or CaH_2, methanol by distillation from magnesium turnings, and both DCE and DCM by distillation from P_2O_5. All reactions were performed under an atmosphere of dry nitrogen. Melting points are uncorrected. Fractional sublimations were performed in an ATS series 3210 three-zone tube furnace, mounted horizontally and linked to a series 1400 temperature control system. Infrared spectra (Nujol mulls, KBr optics) were recorded on a Nicolet Avatar FTIR spectrometer at 2 cm^{-1} resolution. ^1H NMR spectra were run on a Bruker Avance 300 MHz NMR spectrometer, and low-resolution electrospray ionization (ESI) mass spectra were run on a Micromass

(45) Desiraju, G. R. *Angew. Chem., Int. Ed. Engl.* **1995**, *34*, 2311.

(46) (a) Gütlich, P.; Hauser, A.; Spiering, H. *Angew. Chem., Int. Ed. Engl.* **1994**, *33*, 2024. (b) Bousseksou, A.; Molnár, G.; Matouzenko., G. *Eur. J. Inorg. Chem.* **2004**, 4353. (c) Gütlich, P.; Goodwin, H. A. *Top. Curr. Chem.* **2004**, *233*, 1.

Q-TOF Ultima Global LC/MS/MS system. Elemental analyses were performed by MHW Laboratories (Phoenix, AZ).

Preparation of *N*-Ethyl-2,4,6-trifluoropyridinium Triflate, 6. A mixture of ethyl triflate (2.74 mL, 24.0 mmol) and 2,4,6-trifluoropyridine **5** (2.66, 20.0 mmol) was stirred for 16 h at 60 °C to afford a heavy white precipitate. DCE (10 mL) and diethyl ether (35 mL) were added, and the product **6** was filtered off, washed with diethyl ether, and dried in vacuo. Yield, 5.73 g (18.4 mmol, 92%); mp 122−124 °C. IR: 3063 (s), 1673 (vs), 1600 (vs), 1538 (m), 1508 (s), 1424 (w), 1271 (vs), 1228 (s), 1208 (m), 1168 (vs), 1095 (w), 1033 (vs), 881 (m), 759 (w), 639 (vs), 575 (w), 518 (s), 410 (w) cm^{-1}. ^1H NMR (δ, CD_3CN): 7.65 (dd, 2H, $J = 6.89, 2.59$ Hz), 4.57 (qt, 2H, $J = 7.35, 2.72$ Hz), 1.51 (t, 3H, $J = 7.35$ Hz). ^{19}F NMR (δ, CD_3CN): 69.7 (t, 1F, $J = 30$ ppm), 77.7 (d, 2F, $J = 30$ ppm). Anal. Calcd for $C_8H_7F_6NO_3S$: C, 30.88; H, 2.27; N, 4.50. Found: C, 30.83; H, 2.36; N, 4.36.

Preparation of *N*-Ethyl-2,6-diamino-4-fluoropyridinium Triflate, 7. Anhydrous ammonia gas was passed over a solution of **6** (4.70 g, 0.0151 mol) in 50 mL of MeCN at 0 °C for 5−10 min. The yellow mixture was stirred at room temperature for 30 min, and the resulting white precipitate of NH_4F was filtered off. Evaporation of the solvent from the filtrate afforded a white solid that was recrystallized from a 1:5 mixture of MeCN/DCE as off-white flakes of **7**. Yield, 3.34 g (0.0109 mmol, 72%); mp 132−134 °C. IR: 3419 (s), 3361 (s), 3248 (s), 3116 (w), 1672 (s), 1649 (s), 1604 (s), 1548 (w), 1517 (s), 1448 (m), 1339 (m), 1280 (s), 1257 (s), 1226 (s), 1180 (s), 1166 (s), 1091 (m), 1069 (w), 1032 (s), 1015 (m), 811 (s), 793 (w), 761 (w), 642 (s), 598 (w), 580 (w), 573 (w), 515 (m) cm^{-1}. ^1H NMR (δ, CD_3CN): 6.38 (s, 4H), 5.96 (d, 2H, $J = 9.63$ Hz), 3.91 (q, 2H, $J = 7.36$ Hz), 1.31 (t, 3H, $J = 7.36$ Hz). Anal. Calcd for $C_8H_{11}F_4N_3O_3S$: C, 31.48; H, 3.63; N, 13.77. Found: C, 31.83; H, 3.40; N, 13.58.

Preparation of 8-Fluoro-4-ethyl-4*H*-bis[1,2,3]dithiazolo[4,5-*b*:5′,4′-*e*]pyridin-2-ium Trifluoromethanesulfonate, [1a][OTf]. A solution of sulfur monochloride (9.20 g, 0.0681 mol) in 20 mL of MeCN was added to a solution of **7** (5.22 g, 0.0171 mol) in 90 mL of MeCN. The solution was heated at a gentle reflux for 90 min, and the resulting deep blue solution was cooled to room temperature and then at −20 °C for 2 h. The red, microcrystalline precipitate of crude [**1a**][OTf] was filtered off and washed with 4 × 40 mL of hot DCE, 20 mL of CS_2, and 20 mL of DCM, after which the product was dried *in vacuo*. Yield, 5.52 g (0.0129 mol, 75%). Red blocks were isolated by recrystallization from MeCN, mp 291−293 °C. IR: 1512 (s), 1461 (s), 1279 (s), 1239 (s), 1224 (w), 1197 (w), 1121 (w), 1025 (s), 856 (w), 790 (m), 786 (m), 716 (w), 678 (w), 671 (w), 650 (w), 635 (m), 516 (w), 479 (m), 472 (m). Anal. Calcd for $C_8H_5F_4N_3O_3S_5$: C, 22.48; H, 1.18; N, 9.83. Found: C, 22.60; H, 1.23; N, 9.66.

Preparation of 8-Fluoro-4-ethyl-4*H*-bis[1,2,3]dithiazolo[4,5-*b*:5′,4′-*e*]pyridin-3-yl, 1a. Before use, all glassware was soaked overnight in dilute HNO_3, washed with deionized water followed by distilled water, and finally dried at 100 °C overnight. Magnetic stir bars were glass-covered. A sample of [**1a**][OTf] (300 mg, 0.702 mmol) and DMFc (218 mg, 0.668 mmol) were combined in 10 mL of degassed (four freeze−pump−thaw cycles) MeCN at 0 °C. After the mixture was stirred for 2 h at room temperature, the black-green microcrystalline product (α-**1a**) was filtered off and washed with 5 × 10 mL of MeCN. Yield, 155 mg (0.557 mmol, 83%). IR: 1528 (w), 1505 (w), 1438 (s), 1456 (s), 1444 (s), 1351 (w), 1320 (m), 1233 (s), 1190 (w), 1102 (m), 1076 (m), 989 (w), 872 (w), 816 (s), 768 (s), 686 (s), 658 (m), 640 (s), 536 (w), 470 (s), 455 (w). *Radical phase* α-***1a***: Crystals suitable for crystallographic work were obtained by recrystallization of **1a** (250 mg, 0.898 mmol) from 10 mL of degassed (four freeze−pump−thaw cycles) DCE as metallic green needles of α-**1a**. *Dimer phase* β-**1a**: Crystals suitable for crystallographic work, as well as transport property measurements, were obtained by vacuum sublimation of the bulk material at 10^{-4} Torr in a three-zone furnace along a temperature gradient of 120 to 60 °C. This gave pure metallic bronze blocks of β-**1a**. IR: 1528 (s), 1509 (s), 1436 (s), 1328 (s), 1271 (m), 1193 (m), 1168 (s), 1101 (s), 1087 (m), 1073 (m), 872 (w), 835 (m), 764 (s), 713 (m), 661 (s), 615 (w), 574 (w), 522 (w), 473 (s), 424 (w). Anal. Calcd for β-**1a**, $C_7H_5FN_3S_4$: C, 30.20; H, 1.81; N, 15.09. Found: C, 30.35; H, 1.90; N, 15.13.

Cyclic Voltammetry. Cyclic voltammetry was performed using a PINE bipotentiostat, Model AFCClBP1, with scan rates of 50−100 mV s^{-1} on solutions of [**1a**][OTf] in CH_3CN (dried by distillation from P_2O_5 and CaH_2) containing 0.1 M tetra-*n*-butylammonium hexafluorophosphate. Potentials were scanned with respect to the quasi-reference electrode in a single-compartment cell fitted with Pt electrodes and referenced to the Fc/Fc^+ couple of ferrocene at 0.38 V vs SCE. The $E_{pa} - E_{pc}$ separation of the reversible couples was within 10% of that of the Fc/Fc^+ couple.[47]

EPR Spectroscopy. The X-band EPR spectrum of **1a** was recorded at ambient temperature using a Bruker EMX-200 spectrometer; samples of the radical and dimer phase dissolved in degassed CH_2Cl_2 afforded precisely the same spectrum. Hyperfine coupling constants were obtained by spectral simulation using Simfonia[48] and WinSim.

Single-Crystal Crystallography. Crystals of both phases of **1a** were glued to glass fibers with epoxy. X-ray data were collected using ω scans with a Bruker APEX I CCD detector on a D8 three-circle goniometer and Mo Kα ($\lambda = 0.71073$ Å) radiation. The data were scanned using Bruker's SMART program and integrated using Bruker's SAINT software.[49] The structures were solved by direct methods using SHELXS-90[50] and refined by least-squares methods on F^2 using SHELXL-97[51] incorporated in the SHELXTL[52] suite of programs.

High-Temperature Powder Crystallography. A powdered sample (ca. 60 mg) of β-**1a** was loaded into an alumina holder which was rotated and heated to 120 °C in a FUR 1400 furnace under a dynamic atmosphere of helium. X-ray diffraction data were collected on a powder diffractometer with a position-sensitive detector (INEL) using Cu $K\alpha_1$ radiation ($\lambda = 1.5406$ Å). The total 2θ range was 0−112°, measured in steps of 0.029°. The powder diffraction patterns were indexed using DASH 3.01,[53] from which it was evident that the $P2_1/c$ space group of the ambient-temperature structure was retained at 120 °C. Starting with the molecular coordinates for β-**1a** taken from a UB3LYP/6-31G(d,p) geometry optimization, the crystal structure was solved using DASH 3.01. During the initial Rietveld refinement in DASH, a rigid-body constraint was maintained, but the sulfur positions were later released to optimize within the plane of the molecule. These atomic coordinates were then taken into GSAS[54] for a final Le Bail[55] refinement of the unit cell dimensions. Atomic positions obtained from DASH were not further refined in GSAS, as a result of which standard deviations for atomic coordinates are not available. Final refinement indices R_p and R_{wp} are listed in Table 1.

High-Pressure Powder Crystallography. High-pressure diffraction experiments on β-**1a** were performed on the High Energy X-ray Materials Analysis (HXMA) beamline of the Canadian Light

(47) (a) Boeré, R. T.; Moock, K. H.; Parvez, M. *Z. Anorg. Allg. Chem.* **1994**, *620*, 1589. (b) Boeré, R. T.; Roemmele, T. L. *Coord. Chem. Rev.* **2000**, *210*, 369.
(48) *WinEPR Simfonia*, version 1.25; Bruker Instruments, Inc.: Billerica, MA, 1996.
(49) *SAINT*, version 6.22; Bruker Advanced X-ray Solutions, Inc.: Madison, WI, 2001.
(50) Sheldrick, G. M. *Acta Crystallogr. A* **1990**, *46*, 467 SHELXS-90.
(51) Sheldrick, G. M. *SHELXL-97*, Program for the Refinement of Crystal Structures; University of Gottingen: Gottingen, Germany, 1997.
(52) *SHELXTL*, Version 6.12, Program Library for Structure Solution and Molecular Graphics; Bruker Advanced X-ray Solutions, Inc.: Madison, WI, 2001.
(53) David, W. I. F.; Shankland, K.; van de Streek, J.; Pidcock, E.; Motherwell, W. D. S.; Cole, J. C. *J. Appl. Crystallogr.* **2006**, *39*, 910.
(54) Larson, A. C.; Von Dreele, R. B. Report No. LA-UR-86-748; Los Alamos National Laboratory: Los Alamos, NM, 1987.
(55) Le Bail, A.; Duroy, H.; Fourquet, J. L. *Mater. Res. Bull.* **1988**, *23*, 447.

Source, using synchrotron radiation ($\lambda = 0.509176$ Å) and a powdered sample mounted in a diamond anvil cell with low-viscosity (1 cst) polydimethylsiloxane as the pressure-transmitting medium. The diffraction data were collected at room temperature and as a function of *increasing* pressure. A series of data sets from 0 to 1.21 GPa was indexed in DASH, and two of these, collected at 0.65 and 0.98 GPa, were solved, starting from a model radical **1a** derived from a fully optimized UB3LYP/6-311G(d,p) calculation. During the initial Rietveld[56] refinement in DASH, a rigid-body constraint was maintained, but the sulfur positions were later released to optimize within the plane of the molecule. These atomic coordinates were then taken into GSAS for a final Le Bail or Rietveld refinement. Data were refined with fixed atomic positions and isotropic thermal parameters with an assigned value of 0.025. Atomic positions obtained from DASH were not further refined in GSAS, as a result of which standard deviations for atomic coordinates are not available. Final Rietveld indices R_p and R_{wp} are listed in Table 1.

Magnetic Susceptibility Measurements. DC magnetic susceptibility measurements on both phases of **1a** were performed over the range 2−400 K on a Quantum Design MPMS SQUID magnetometer operating at $H = 1000$ Oe. Diamagnetic corrections were made using Pascal's constants,[57] and the data for α-**1a** were modeled using a molecular-field modified Heisenberg 1D AFM $S = {}^1/_2$ chain fit function.[58]

Conductivity Measurements. High-pressure/temperature conductivity experiments on both phases of **1a** were carried out with 1000 ton cubic anvil press[59] using pyrophyllite ($Al_4Si_8O_{20}(OH)_4$) as the pressure-transmitting medium. Sample pressure was determined from previous calibrations[59,60] of the applied hydraulic load against pressures of structure transformations in standards at room temperature (Bi I−II at 2.46 GPa and III−VII at 7.7 GPa, Tl I−III at 3.70 GPa, and ZnTe I−I′ at 6.6 GPa and I′−II at 8.9 GPa). The pressure cell design[61] was modified to include a Nb furnace, and Pt disk electrodes contacted the precompacted powder samples contained in a boron nitride ($\sigma_{BN} = 10^{-11}$ S cm^{-1}) cup. Contacts to the Pt disks were made with Re/W (97%/3%) wires. Four-wire AC (Solartron 1260 impedance analyzer) resistance measurements were made at a frequency of either 1 or 100 kHz. The contiguous disk-shaped sample was extracted from the recovered pressure cell, and the sample geometry was measured to convert resistance to conductivity.

Molecular Electronic Structure Calculations. All DFT calculations were performed with the Gaussian 09W suite of programs,[62] using the (U)B3LYP hybrid functional and polarized, split-valence basis sets with double-ζ (6-31G(d,p)) and triple-ζ (6-311G(d,p)) functions. Full geometry optimization was invoked for the assembly of the model of **1a** used as the starting point in the powder diffraction work. For the calculation of the electronic energies of singlet σ-dimer and ^3B_u radical pairs for **1** and **2** ($R_1 = R_2 = H$), full geometry optimization within the confines of C_{2h} symmetry was invoked, with only the values of q and r defined in Figure 15 being constrained.

Acknowledgment. We thank the Natural Sciences and Engineering Research Council of Canada (NSERCC) for financial support. We also acknowledge the NSERCC for Canada Graduate Scholarships to S.M.W. and L.E.D., a Vanier Graduate Scholarship to K.L., and the Government of Canada for a Tier I Canada Research Chair to J.S.T. Synchrotron work at the Canadian Light Source was made possible by support from the NSERCC, NRC, CIHR, and the University of Saskatchewan.

Supporting Information Available: Complete refs 15a and 62; details of X-ray crystallographic data collection and structure refinement, tables of atomic coordinates, bond distances and angles, anisotropic thermal parameters, and hydrogen atom positions in CIF format; FTIR spectra for the α- and β-phases of **1a**; details of magnetic data fitting and exchange energy calculations for α-**1a**. This material is available free of charge via the Internet at http://pubs.acs.org.

JA106768Z

(56) Rietveld, H. M. *J. Appl. Crystallogr.* **1969**, *2*, 65.
(57) Carlin, R. L. *Magnetochemistry*; Springer-Verlag: New York, 1986.
(58) Estes, W. E.; Gavel, D. P.; Hatfield, W. E.; Hodgson, D. J. *Inorg. Chem.* **1978**, *17*, 1415.
(59) Secco, R. A. *Can. J. Phys.* **1995**, *73*, 287.
(60) Secco, R. A.; Liu, H.; Imanaka, N.; Adachi, G. *J. Mater. Sci. Lett.* **2001**, *20*, 1339.
(61) Wang, D.; Mookherjee, M.; Xu, Y.; Karato, S. *Nature* **2006**, *443*, 977.
(62) Frisch, M. J.; et al. *Gaussian 09*, Revision A.02; Gaussian, Inc.: Wallingford, CT, 2009.